A mouse-human phase 1 co-clinical trial of a protease-activated fluorescent probe for imaging cancer

A Mouse-Human Phase I Co-Clinical Trial of the Protease-Activated Fluorescent Probe LUM015 for Imaging Cancer

Authors: M. J. Whitley[1,2], D. M. Cardona[3], A. L. Lazarides[4], I. Spasojevic[5,6], J. M. Ferrer[7], J. Cahill[8], C.L. Lee[8], Matija Snuderl[9‡], D.G. Blazer III[10], S. E. Hwang[10], R. A. Greenup[10], P. J. Mosca[10], J. K. Mito[1,2], K. C. Cuneo[8], N. A. Larrier[8], E. K. O'Reilly[11], R. F. Riedel[5], W. C. Eward[12], D. B. Strasfeld[7], D. Fukumura[9], R. K. Jain[9], W. D. Lee[7], L. G. Griffith[13], M. G. Bawendi[14], D. G. Kirsch[1,8*†] and B. E. Brigman[12†]

Affiliations:

[1]Department of Pharmacology and Cancer Biology, Duke University Medical Center, Durham, North Carolina 27710, USA.

[2]Medical Science Training Program, Duke University Medical Center, Durham, North Carolina 27710, USA.

[3]Department of Pathology, Duke University Medical Center, Durham, North Carolina 27710, USA.

[4]School of Medicine, Duke University Medical Center, Durham, North Carolina 27710.

[5]Department of Medicine, Duke University Medical Center, Durham, North Carolina 27710, USA.

[6]PK/PD Core Laboratory, Duke Cancer Institute, Duke University Medical Center, Durham, North Carolina 27710, USA.

[7]Lumicell, Inc., Wellesley, Massachusetts 02481, USA.

[8]Department of Radiation Oncology, Duke University Medical Center, Durham, North Carolina 27710, USA.

[9]Edwin L. Steele Laboratory, Department of Radiation Oncology, Massachusetts General Hospital and Harvard Medical School, Boston, Massachusetts 02114, USA.

[10]Department of Surgery, Duke University Medical Center, Durham, North Carolina 27710, USA.

[11]Duke Translational Medicine Institute, Regulatory Affairs Group, Duke University Medical Center, North Carolina 27710, USA.

[13]Department of Orthopaedic Surgery, Duke University Medical Center, Durham, North Carolina 27710, USA.

[12]Department of Biological Engineering, Massachusetts Institute of Technology, Cambridge, Massachusetts 02142, USA.

[14]Department of Chemistry, Massachusetts Institute of Technology, Cambridge, Massachusetts 02142, USA.

*Corresponding author. E-mail: david.kirsch@duke.edu

†Co-Senior Authors

‡Current Address: Department of Pathology, NYU Langone Medical Center, New York, New York 10016, USA.

One Sentence Summary: A first-in-human Phase I clinical trial of the PEGylated, protease-activated fluorescent imaging probe, LUM015, shows tumor-specific fluorescence at a safe and tolerable dose in humans.

Abstract:

Local recurrence is a common cause of treatment failure for patients with solid tumors. Intra-operative detection of microscopic residual cancer in the tumor bed could be used to decrease the risk of a positive surgical margin, reduce rates of re-excision, and tailor adjuvant therapy, all of which may contribute to improved disease control. Here, we use a protease–activated fluorescent imaging probe, LUM015, to detect cancer *in vivo* in a mouse model of soft tissue sarcoma (STS) and *ex vivo* in a first-in-human Phase I clinical trial. In mice, intravenous injection of LUM015 labeled tumor cells and residual fluorescence detected within the tumor bed predicted local recurrence. In fifteen patients with STS or breast cancer, intravenous injection of LUM015 prior to surgery was well tolerated. Imaging of resected human tissues showed that fluorescence from tumor was significantly higher than fluorescence from normal tissue. Comparison of LUM015 biodistribution and metabolism in mouse and human subjects revealed similar pharmacokinetic profiles for this PEGylated imaging probe. The major fluorescent LUM015 metabolite was determined to be Cy5-Lysine. Tissue concentrations of LUM015 and its metabolites demonstrated that LUM015 is selectively distributed to tumors where it is activated by proteases to establish tumor to normal contrast. Experiments in mice with a constitutively active PEGylated fluorescent imaging probe support a model where tumor-selective probe distribution is a determinant of increased fluorescence in cancer. These co-clinical studies suggest that the tumor-specificity of protease-activated imaging probes, such as LUM015, is significantly dependent on both biodistribution and protease-activation. These results support future clinical trials of LUM015 in which intraoperative imaging of the tumor bed is compared to surgical margin histopathology.

Main Text:

Introduction

Surgical resection is the primary treatment modality for most solid tumors diagnosed before metastatic spread. In patients with soft tissue sarcoma (STS) of the extremity and breast cancer, organ-sparing surgery alone prevents local recurrence in approximately two-thirds of patients (*1-3*). With standard histopathological margin analysis, there is no way to identify which patients will recur after surgery alone and therefore, most patients receive adjuvant radiation therapy. Although radiation therapy significantly improves local recurrence-free survival for the entire population (*1-4*), the majority of patients, who would have achieved local control with surgery alone, derive no benefit from adjuvant radiation therapy. Despite advances in the delivery of radiation therapy to decrease morbidity (*5*), radiation therapy can cause fibrosis, swelling, joint stiffness, and secondary malignancy. Therefore, a method to identify patients with microscopic residual cancer in the tumor bed could stratify patients for adjuvant therapy.

The risk of residual cancer remaining in the tumor bed is often inferred by the pathologist's evaluation of the excised surgical margin. If tumor cells are present at the surface of the excised margin, which is termed a positive margin, then a patient has an increased risk of local recurrence (*2, 6*). The current standard of care for intraoperative margin assessment consists of gross evaluation and histopathological examination of frozen sections of the tissue margin using light microscopy. Assessment of frozen sections in the intraoperative period is limited by time and prone to sampling error, leading to false negative results in up to 23% of cases (*7*). Importantly, this method uses the presence or absence of tumor cells on the margins of the resected tissue as a surrogate for what may be present in the tumor bed. An intraoperative technique to accurately identify microscopic residual disease within the tumor bed could be used

to decrease the risk of a positive surgical margin, reduce the rate of re-resection, and tailor adjuvant therapy.

An emerging approach to detect microscopic residual disease within the tumor bed is to use optical imaging with fluorescent imaging probes. Non-specific fluorescent imaging probes like methylene blue and indocyanine green (ICG) can provide contrast between tumor and normal tissues and are currently in clinical trials. The tumor-to-background ratio (TBR) with these imaging agents ranges from 1.2-2.4 in mouse and human studies (*8, 9*). To increase the TBR, targeted fluorescent probes have also been developed. These include fluorophores conjugated to peptides or antibodies that bind to receptors highly expressed on tumor cells (*10-12*) as well as activatable probes that are optically silent until cleaved by proteases that are overexpressed by tumors (*13*). Many proteolytic enzymes are upregulated intracellularly in cancer cells and extracellularly in the tumor microenvironment where they may play a role in tumor progression and spread (*14*). Cathepsin proteases are a specific family of proteases that are highly upregulated in a variety of cancers when compared with normal tissues (*15*).

Previously, we utilized the *LSL-Kras*$^{G12D/+}$*; p53*$^{Flox/Flox}$ (KP) and *Braf*$^{Ca/+}$*; p53*$^{Flox/Flox}$ (BP) mouse models of STS to develop a wide field-of-view imaging system that detects fluorescence (*16*). Because cathepsin proteases are preferentially expressed in STS compared to skeletal muscle, we used commercially available cathepsin-activated fluorescent probes to specifically label the tumor cells. Residual fluorescence in the tumor bed correlated with local recurrence and we demonstrated that image-guided surgery improved outcomes for mice with positive residual fluorescence (*16*). This intraoperative imaging system has also been utilized to detect residual disease within the tumor bed of canine patients with spontaneous tumors (*17*).

To translate this work into the operating room, we explored the use of LUM015 (Lumicell, Inc., Wellesley, MA), a PEGylated protease-activated deep red fluorescent imaging probe containing a Cy5 fluorophore linked to a quencher by a polypeptide that contains an Arginine-Lysine protease cleavage site. In this state, the probe is optically inactive but upon cleavage, the quencher is released so that Cy5 fluorescence can be detected (**Supplementary Figure 1**). Preclinical toxicity studies of LUM015 were performed in rats and indicated a wide margin of safety.

We report here a first-in-human Phase I trial of LUM015 to test the safety of the probe in patients undergoing surgery for STS and breast cancer and present pharmacokinetic data on LUM015 and its metabolites as well as imaging data of excised tumor and normal tissues. Co-clinical studies in mice were conducted to optimize the dose and timing of LUM015 administration and to investigate the *in vivo* mechanisms of tumor-specificity. Our studies support further clinical development of LUM015 in clinical trials with intra-operative imaging of the tumor bed.

Results

LUM015 fluorescently labels tumor cells in mice

To test the specificity of the protease-activated probe LUM015 for tumor cells, we administered 3.5 mg/kg LUM015 by tail vein injection into sixteen mice with primary STS in the left lower extremity. Six hours later, we resected the STS and normal muscle from the contralateral leg. Fluorescence imaging of the resected tissues revealed mean tumor fluorescence which was 4.8 times higher than the mean normal muscle fluorescence (**Figure 1A, B; P<0.006**). We also

tested LUM015 in a mouse model of breast cancer and found that the mean tumor fluorescence was 3.6 times higher than the mean normal muscle fluorescence (**Supplementary Figure 2**).

Because tumors consist of cancerous and stromal cells, such as macrophages, lymphocytes, and endothelial cells, we next investigated whether LUM015 labeled tumor cells and/or stromal cells. For these experiments we utilized genetically engineered mice with a Cre-activated yellow fluorescent reporter allele (*Rosa26-LSL-YFP*) so tumor cells express YFP. After primary sarcomas developed, we injected the mice with LUM015 (n=3) or phosphate buffered saline (PBS) as a control (n=2). Six hours later, the tumors were resected, digested into single-cell suspensions, and analyzed by flow cytometry. Tumors resected from mice injected with LUM015 had a significantly higher proportion of Cy5+ fluorescent cells compared controls (**Figure 1C, D**). Over 60% of the LUM015-labeled cells were YFP+ tumor cells and less than 10% were CD11b+ tumor associated monocytes and macrophages (**Figure 1C, E**), which suggests that the majority of Cy5 labeled cells are tumor cells. Additionally, we found that the proportion of Cy5 labeled cells was higher in the YFP+ tumor cell population than in the CD11b+ population (**Supplementary Figure 3**).

Having demonstrated that LUM015 fluorescently labels sarcoma cells, we next utilized a mouse model of STS with marginal resection to determine if residual fluorescence in the tumor bed after surgical removal of the tumor predicted local recurrence. The presence of residual fluorescence within the tumor bed was determined intraoperatively as fluorescence exceeding 80% of the minimum signal from the excised tumor as we described previously (**Supplementary Figure 4)** (*16*). After imaging the tumor bed, the surgical wound was closed and the mice were monitored for local recurrence. All of the mice with positive residual fluorescence developed local recurrence of their tumors within 70 days of surgery. In comparison, only one-third of the

mice with negative residual fluorescence developed local recurrence with 200 total days of follow-up (**Figure 1F**).

A first-in-human Phase I clinical trial of LUM015

After demonstrating that LUM015 selectively labeled sarcoma and breast cancer in mice and after completing pre-clinical toxicity studies in rats, we performed a first-in-human Phase I clinical trial of LUM015. This trial enrolled fifteen patients, twelve with STS and three with breast cancer. The tumor subtypes, grade, size and anatomic locations are described in **Table 1**. LUM015 was administered to six patients at a 0.5 mg/kg dose, six patients at a 1.0 mg/kg dose, and three patients at a 1.5 mg/kg dose according to a modified 3+3 design. These human doses were chosen based on the estimated effective dose of 3.5 mg/kg in mice, which often corresponds to a lower effective dose in humans due to differences in the ratio of body surface area to body weight (*18*). Surgery to remove the tumors immediately followed by *ex vivo* fluorescence imaging of the resected specimens occurred either the same day as probe injection (at ~6 hours) or the following day (at ~30 hours). Tissue samples imaged *ex vivo* were biopsied for subsequent histological analysis. Patients treated with neoadjuvant radiation therapy were included in the study based on our previous data that radiation therapy does not alter the fluorescence from protease-activated imaging probes in a mouse model of STS (*19*). LUM015 was well tolerated by study subjects and no adverse pharmacological activity (APA), hypersensitivity reactions, or other significant adverse events occurred during the study (**Supplementary Table 1**). All subjects experienced green chromaturia, which was expected based on the blue color of LUM015. Two of 12 sarcoma patients had wound healing complications, which is within the expected range for this patent population. These events were not considered related to LUM015. Both of these patients had received pre-operative radiation

therapy, which is known to delay wound healing in soft tissue sarcoma patients(*20*). Of note, the tissue imaged for patient ten did not include tumor, and therefore this patient is excluded from analyses of tumor imaging.

Co-clinical pharmacokinetic studies

Blood samples were collected from mice and humans at regular intervals following intravenous (IV) administration of LUM015 and LC-MS/MS was used to measure the plasma concentration of LUM015 at these time points. Summary pharmacokinetic parameters suggesting a linear dose response in humans are reported in **Supplementary Table 2**. We observed that the LUM015 plasma clearance profiles from mice and humans injected with a 1.5 mg/kg dose of LUM015 are similar (**Figure 2A**). Based on these data, as well as the finding that tumor fluorescence in the first six humans imaged at 30 hours was lower than fluorescence measured in mice imaged at 6 hours (**Figure 2B**), the imaging time point was shortened to 6 hours after LUM015 administration for the remainder of the Phase I trial. In both mice and humans, we found that absolute tumor fluorescence was significantly higher when measured 6 hours after LUM015 administration compared to 30 hours (**Figure 2B**). In contrast, we did not find a significant effect of imaging time on the tumor to normal tissue fluorescence ratio in humans or mice (**Figure 2C**). We also examined the effect of dose on tumor to normal tissue fluorescence ratios in mice and humans and found that the fluorescence ratio measured in humans administered the highest LUM015 dose (1.5 mg/kg) was significantly higher than in the two lower dose cohorts (**Figure 2D**). However, we did not observe a significant difference in the fluorescence ratio between the 1.5 mg/kg and 3.5 mg/kg dose cohorts in mice.

LUM015 fluorescence is tumor-selective in STS and breast cancer patients

To determine if preoperative administration of IV LUM015 results in tumor-specific fluorescence, we compared the absolute tumor fluorescence with the absolute fluorescence from adjacent normal tissue. The presence or absence of cancer in the samples was confirmed by subsequent histological analysis by a pathologist blinded to the imaging data (**Supplementary Table 3**). Normal muscle, adipose, or breast tissue from the margin of tissue resected around the tumor was used for the normal tissue comparison unless otherwise noted in **Supplementary Table 3**. For each patient, we imaged 1 to 6 tumor and normal tissue sites that were histologically confirmed and the mean fluorescence value is reported. We found that tumor fluorescence was significantly higher than matched normal tissue fluorescence and the mean tumor to normal fluorescence ratio was 4.1 (**Figure 3A**). Furthermore, we found that the distribution of absolute tumor fluorescence values was significantly different from the distributions of absolute muscle and adipose tissue fluorescence values (**Figure 3B**). Two representative examples of *ex vivo* imaging from a patient with a high grade undifferentiated pleomorphic sarcoma (UPS) of the thigh and a patient with a high grade invasive ductal carcinoma (IDC) of the breast are shown (**Figure 3C, D**).

LUM015 forms two different optically active metabolites

The protease-activated LUM015 fluorescent probe consists of a fluorescence quencher molecule (QSY21, Life Technologies) attached via a Gly-Gly-Arg-Lys peptide to a 20 kD PEG at the C-terminus and a Cy5 fluorophore covalently linked to the amino group of lysine (**Figure 4A**). The hydrodynamic radius of 20 kD PEG has been reported as between 3 to 3.5 nm (*21*). For this study, LUM015 was dissolved in PBS and the measurement was carried out at 37ºC to mimic physiologic conditions. LUM015 was designed with a canonical arginine-lysine cathepsin

protease cleavage site, yielding an optically inactive Fragment 1 containing the quencher and an optically active Fragment 2, containing the Cy5 fluorophore and PEG. Additional cleavage of LUM015 or Fragment 2 at the C-terminus of lysine yields optically active Fragment 3, consisting of the Cy5 fluorophore attached only to lysine (**Figure 4A**). Analysis of LUM015, Fragment 2, and Fragment 3 standards using high pressure liquid chromatography coupled with a fluorescence detector (HPLC-FD) revealed a distinct fluorescent peak for each fragment (**Figure 4B**). The low-level fluorescence detected from the LUM015 standard is due to approximately 1% of Cy5 fluorescence not being absorbed by the fluorescence quencher. We observed that the molar fluorescence intensity of Fragment 3 was greater than that of Fragment 2. HPLC-FD analysis of patient plasma samples showed a strong peak corresponding to Fragment 3 as well as a smaller peak representing Fragment 2 and uncleaved LUM015 (**Figure 4C**). Human plasma profiles of Fragment 3 were generated from HPLC-FD analysis and showed Fragment 3 levels increasing the first 8 hours after injection followed by clearance at a slower rate (**Figure 4D**). To determine if formation of Fragment 3 occurs in a tumor-specific manner, we injected mice with and without primary STS with LUM015 and measured plasma Fragment 3 concentrations at several time points after administration. At one hour, plasma levels of Fragment 3 peaked in mice with tumors, but by two hours, plasma levels decreased to a level similar to mice with no tumor, suggesting that Fragment 3 was appreciably produced in non-tumor tissues (**Figure 4E**). Furthermore, we incubated LUM015 with mouse blood, muscle, tumor, liver and kidney tissues *in vitro* to measure tissue-specific LUM015 metabolism (**Supplementary Figure 5**). We found that in tumor tissue, the majority of LUM015 was metabolized whereas in blood, muscle, liver and kidney tissue, half or more the probe remained uncleaved. Both Fragment 2 and Fragment 3

were measured in all tissues, but Fragment 2 was the predominant cleavage product in this *in vitro* experiment.

The roles of biodistribution and protease activation in tumor fluorescence

After determining that Fragment 3 was the major LUM015 metabolite in human plasma, we measured the concentration of Fragment 3 as well as LUM015 and Fragment 2 in human tissues in addition to a cohort of 18 mice injected with 1.5 mg/kg LUM015 and imaged at a 6 hour imaging time point. The tumor concentration of Fragment 3 was significantly correlated with tumor fluorescence in mice and humans (**Figure 5A.**) A similar analysis of Fragment 2 in mouse and human samples showed a weaker correlation with tissue fluorescence (**Supplementary Figure 6A**). To measure the contribution of probe activation by proteases to tumor-selective fluorescence, we calculated the fraction of LUM015 and its metabolites that were present in the optically active state for each mouse sample. In the mouse cohort, sarcomas had a fraction of activated probe of 0.38 +/- 0.03 which was approximately 50% higher than normal muscle at 0.26 +/- 0.03 ($P<0.01$, *t*-test) (**Figure 5B**). In human tumor samples imaged at 6 hours, tumors had a fraction of activated probe of 0.26 +/- 0.06, which was approximately 60% higher compared to normal tissues at 0.16 +/- 0.02 (**Supplementary Figure 6B**), but this difference did not reach statistical significance in this sample ($P=0.1$, *t*-test). In the human samples imaged at 30 hours, there was no difference between normal and tumor tissue in the fraction of activated probe (**Supplementary Figure 6B**). In the mouse STS cohort and in the human STS patients at the 6 hour imaging cohort with normal muscle available for comparison (Patients 8, 11, 12, 13, and 14), tumor:muscle fluorescence ratios were correlated with the corresponding activation ratio ($r^2= 0.44$ for human samples and $r^2=0.52$ for mouse samples), however this correlation reached statistical significance only for the mouse samples (**Figure 5C**). To measure the

contribution of biodistribution to tumor-selective fluorescence, the total concentration of LUM015, Fragment 2, and Fragment 3 ([Total Probe]) was determined for each mouse and human sample (**Figure 5D)**. In the mouse cohort, sarcomas had a [Total Probe] of 221 +/- 34, which was approximately four times that of normal muscle at 56 +/- 6 ($P<0.0001$, *t*-test). In the human STS cohort, sarcomas had a [Total Probe] of 154 +/- 38 which was approximately 100% higher compared to normal tissues at 72 +/- 13 ($P=0.08$, *t*-test). Therefore, we tested whether tissue fluorescence correlated with total probe concentration in mouse and human sarcomas. We found the two variables to have a significant positive correlation in the mouse cohort, the human STS cohort, and the overall human dataset (**Figure 5E, Supplementary Figure 6E**). These findings suggested that tumor-selective distribution of LUM015 is a critical determinant of tumor to normal fluorescence ratios which is further enhanced by tumor-specific protease activation. To image tumors with a probe that does not require protease activation, we injected STS-bearing mice with either LUM015 or LUM033 (Lumicell, Inc.), a constitutively active fluorescent imaging probe identical to Fragment 2. We imaged resected tissues from these mice and found a tumor to normal tissue fluorescence ratio of 8 +/- 2 for LUM015 and 4 +/- 1 for LUM033 ($P<0.05$) (**Figure 5F**). Therefore, protease activation may serve to double the level of tumor to normal contrast that is achieved by tumor-selective biodistribution alone.

Since biodistribution is one of two major determinants of tumor-specific fluorescence measured after administration of LUM015, we used immunofluorescence and immunohistochemistry techniques to further examine the distribution of LUM015 to tumor and normal tissues. As a control for immunofluorescence, we used formalin fixed paraffin embedded (FFPE) sections of tumor tissue from a human sarcoma patient not injected with LUM015 (**Figure** 6A). In contrast to the negative control, immunofluorescent staining for PEG on FFPE

sections of tumors from patients who had been injected with LUM015 showed a positive signal (**Figure 6A**). We also identified a breast cancer sample from patient 15 with areas of tumor and adjacent normal tissue. PEG immunofluorescence staining of this section showed PEG signal localized to areas of tumor with less intense staining in areas of adjacent normal tissue (**Figure 6B**). Areas adjacent to tumor containing a lymphocytic infiltrate were also negative for PEG staining. To quantify the intensity of PEG staining in tumors and matching normal tissues from humans injected with LUM015, we performed immunohistochemical staining for PEG on FFPE normal and tumor tissues. We found that the intensity of PEG staining was less in normal muscle tissues and in normal breast tissues compared to sarcomas and breast cancer, respectively (**Figure 6C**). One normal tissue sample and one tumor tissue sample from each patient was scored for intensity of PEG staining by two independent, blinded reviewers, revealing that the intensity of PEG staining is significantly higher in tumor tissues when compared to normal tissue (**Figure 6D**). These results for PEG staining, together with the quantification of LUM015 and its metabolites, suggest that tumor-selective distribution of LUM015 may serve to delineate the tumor margin while protease activation intensifies the contrast between tumor and normal tissue types.

Discussion

There is an unmet need for a real-time method to determine the presence of microscopic residual cancer within the tumor bed at the time of surgery, which could reduce the need for re-resection, lower the rates of local recurrence, and personalize adjuvant therapy. A particularly attractive approach to detect residual disease is fluorescence imaging, because it can be functionally and/or molecularly targeted and provide cellular resolution with penetration depths of up to several millimeters (*10*). Although non-specific probes like ICG can preferentially accumulate in cancer

to provide fluorescent contrast between tumor and normal tissues, the tumor to normal tissue ratio is approximately 2 (*9*). To try to increase the contrast between tumor and normal tissues targeted probes have been utilized that consist of a tumor-specific peptide or antibody conjugated to a fluorophore (*11, 12*). Protease-activated probes may provide increased tumor to normal contrast as they are designed to be optically inactive until cleaved by proteases that are highly expressed in tumors, like cathepsin proteases and matrix metalloproteases (MMPs) (*13, 22-24*). Many of these probes have been developed and tested in preclinical models, but to date, there is no information on the use of these probes to image human cancers and the relative importance of protease-activation versus biodistribution for achieving tumor to normal tissue contrast has not been investigated.

We show here that the PEGylated, protease-activated probe LUM015 specifically labels tumors in a mouse model of STS as well as in humans with STS and breast cancer. Specifically, we injected LUM015 into genetically engineered mice with primary sarcomas to determine a tumor to normal tissue fluorescence ratio of 4.8, which is higher than the TBR reported for several non-specific and tumor-targeted probes (*9, 11, 25, 26*). Flow cytometry studies of whole tumors from LUM015-injected mice showed that the majority of fluorescently labeled cells were tumor cells and less than one-tenth were tumor associated monocytes and macrophages. The labeling of tumor-associated macrophages likely occurs because these cells also express high levels of proteases (*27*) and the intraoperative identification and removal of these cells may, in fact, be beneficial to patients as these cells are associated with tumor progression and metastasis (*28, 29*). Importantly, in a model of sarcoma resection in mice injected with LUM015, residual fluorescence within the tumor bed was highly predictive of local recurrence, suggesting that this intraoperative imaging system could be useful to guide surgery and tailor adjuvant therapy.

In a first-in-human Phase I trial of LUM015 in patients undergoing surgical resection of STS or breast cancer we found that the PEGylated probe is safe and well-tolerated at a dose that allows for detection of tumor-specific fluorescence. We observed that the plasma clearance profile of LUM015 in humans is similar to that observed in mice. Based on the principles of allometric scaling, we expected that the clearance rate would be significantly slower in humans (*30, 31*), so that a greater interval of time between LUM015 administration and tumor resection would be required to allow for optimal tumor to normal tissue contrast. Our results are consistent with findings that standard allometric scaling does not accurately predict human pharmacokinetic parameters for PEGylated compounds (*32*). Based on this information, we modified the Phase I clinical trial to include imaging at a six-hour time point, which similar to the mouse experiments, resulted in higher tumor fluorescence in human cancers than imaging at 30 hours. Although imaging at a later time point does diminish the absolute strength of the fluorescent signal from tumors, this does not appreciably affect the tumor to normal tissue contrast. Therefore, in a clinical scenario where surgery for an already injected patient is delayed for one day, re-administration of LUM015 may not be necessary. Patients injected with the highest LUM015 dose tested, 1.5 mg/kg, had the largest tumor to normal fluorescence ratio, but this observation needs to be validated in future clinical trials with a larger sample size.

Consistent with data in mice with primary sarcomas and dogs with spontaneous tumors (*17*), when patients with STS or breast cancer were injected with LUM015 prior to surgery, we found tumor tissue fluorescence measured *ex vivo* to be significantly higher than fluorescence measured from adjacent normal tissues. Across all patients, we find the distribution of tumor fluorescence values to be significantly different from the distribution of muscle and adipose fluorescence values. This suggests that with a larger cohort of patients, a range of normal tissue

fluorescence values could be determined that might define an absolute threshold to identify cancer. It is important to note that this study included patients with both sarcoma and breast cancer, and that within these tumors, different subtypes were included. A tumor to normal tissue fluorescence ratio of greater than 1 was measured in twelve of fourteen patients, indicating that LUM015 may be effective for fluorescent labeling of many different types of cancer.

LUM015 was designed with a canonical cathepsin cleavage site consisting of two basic residues, arginine-lysine, to allow for enhanced cleavage and activation in tumors which often have higher expression of cathepsin proteases when compared to normal tissues (*14, 33*). Cleavage at this site results in the formation of optically active Fragment 2, which retains the Cy5 fluorophore and the 20 kD PEG. Further cleavage at the peptide bond linking lysine to the PEG moiety, results in the formation of a distinct optically active metabolite Fragment 3 that lacks PEGylation. We found Fragment 3 to be the major LUM015 metabolite *in vivo* with only minimal amounts of Fragment 2 in human plasma and tissue. This suggests that, in humans, Fragment 3 is either produced more readily than Fragment 2 from uncleaved LUM015, or that any Fragment 2 that is formed is quickly cleaved to yield Fragment 3. Interestingly, using mice we found that the generation of Fragment 3 *in vivo* does not require the presence of cancer. Indeed, we showed that in mice, Fragment 3 can be formed in isolated blood, muscle, liver, and kidney. In primary sarcomas generated in mice, the extent of probe activation at 6 hours after LUM015 injection is 1.5 times higher than in normal tissues. Furthermore, there is a significant correlation between tumor: normal fluorescence and probe activation ratios with an r^2 value of 0.52. In the human sarcoma cohort, the extent of probe activation at 6 hours after LUM015 injection is 1.6 times higher than in normal tissue and the correlation between tumor: normal fluorescence and probe activation ratios yields an r^2 value of 0.44. Although the data from the

human cohort does not reach statistical significance in this relatively small sample, it follows the trends found in the larger mouse cohort. These data suggest that protease activation does not fully account for the tumor to normal fluorescence ratio of 5.2 measured in patients imaged at the 6 hour imaging time point and therefore, indicates that additional factors may contribute to tumor-selective fluorescence.

Tissue measurements of LUM015 and its metabolites showed that biodistribution was an important factor in tumor-selective fluorescence. The absolute concentration of Fragment 3 as well as the total concentration of LUM015 within the human tissues was highly correlated with tissue fluorescence. This was consistent with the findings in mice. We also found a significant difference between the concentration of LUM015 and its metabolites (total probe) in human tumor tissues compared to normal tissue. At the 6 hour imaging time point, the concentration of probe was 2.2 times higher in tumors than in normal tissues. In the mouse sarcoma cohort, the concentration of total probe was 3.9 times higher in tumors. Furthermore, using immunohistochemistry and immunofluorescence, we found staining for the PEG moiety of LUM015 to be more intense in tumor tissues than in normal tissues. Taken together, these data suggest that LUM015 selectively accumulates in tumors, likely via the enhanced permeability and retention (EPR) effect. EPR describes the preferential distribution of macromolecules to tumors due to extravasation through leaky tumor vasculature and poor lymphatic drainage, which increases the delivery of large molecules into the tumor microenvironment and slows the rate of clearance from tumors (*34*, *35*). The results of this co-clinical study support a model in which protease-activated probes, like LUM015, are selectively delivered to tumor tissues where they are cleaved and activated. Consistent with this model, we found that administration of a constitutively active fluorescent probe to tumor-bearing mice resulted in a 50% decrease in the

tumor to normal tissue fluorescence ratio when compared to LUM015. Therefore, tumor-specific protease activation serves to enhance the contrast that is established via differential distribution, suggesting that by targeting the tumor via both mechanisms simultaneously, a larger tumor to normal contrast is achieved.

By understanding this cooperative mechanism of tumor-specific fluorescence, we may be able to better identify patients with cancer, who will benefit from intraoperative image-guided surgery with LUM015. We observed a large spread of absolute tumor fluorescence values among humans and this was even present in primary STS-bearing mice with primary tumors initiated by the same genetic mutations. This suggests that, even among tumors of the same subtype, differences in tumor vasculature and protease activity may lead to varying tumor fluorescence values from human to human. The ability to detect these differences before surgery may allow the surgeon to determine whether LUM015 will be an effective tool for a specific patient. It is possible that the extent of tumor-selective probe distribution may correlate with contrast-enhancement of the tumor us MRI or CT. Furthermore, assays could be developed to detect protease activity in tissues obtained during routine diagnostic biopsies.

This work presents a first-in-human Phase I clinical trial of an intravenously administered, protease-activated fluorescent intraoperative imaging probe. We have shown that LUM015 is safe for use in humans and generates tumor-specific fluorescence. These studies support future clinical trials of LUM015 utilizing intra-operative imaging of the tumor bed and comparing imaging results with histopathology. Our co-clinical studies in mice and humans reveal that pharmacokinetic and pharmacodynamic parameters are conserved across species, which may aid in in the translation of other preclinical imaging agents for human use. Finally, we have found that tumor-selective probe distribution and protease activation are significant

determinants of the tumor to normal contrast created by protease-activated fluorescent imaging probes.

Materials and Methods

Human Study Design

The primary objective of the single institution, open-label, nonrandomized Phase I trial was to determine a safe and recommended dose of LUM015 that labels tumors. Secondary objectives included obtaining *ex vivo* imaging information of the tumor and any adjacent normal appearing tissue as well as collecting pharmacokinetic/pharmacodynamic information regarding LUM015 when administered intravenously in patients. Patients with the diagnosis of soft tissue sarcoma or breast cancer scheduled for tumor resection at Duke University Medical Center were included. Twelve patients with soft tissue sarcoma and three patients with breast cancer were enrolled (**Table 1**). The sample size was determined based on a modified 3+3 dose escalation design to provide information on the relationship between dose and fluorescence signal while observing patients for APA. No outliers were excluded in this study. Informed consent was obtained from each patient and the study was approved by the Duke University School of Medicine and Copernicus Institutional Review Boards. The study was also run under an Investigational New Drug (IND) application filed with the Food and Drug Administration (FDA). A Safety Monitoring Committee was formed to protect the rights, safety, and welfare of participants and additional monitoring occurred via the Duke Cancer Institute (DCI) Safety Oversight Committee.

A safety evaluation consisting of history & physical exam, vital signs, electrocardiogram (ECG), blood and urine laboratory studies, and pulmonary function tests (PFTs) were conducted prior to peripheral intravenous (IV) administration of LUM015 at three predetermined doses: 0.5 mg/kg, 1.0 mg/kg, or 1.5 mg/kg. The LUM015 injection was administered either the day before

or on the morning of surgery. LUM015 was supplied free-of-charge from Lumicell Inc. Safety evaluations during the 24-hour period after IV injection consisted of vital signs, ECGs, blood and urine laboratory studies and documentation of any APA. APA was defined as any functional effect on the major physiological systems that is at least probably attributable to LUM015. Laboratory studies and APA evaluation were performed again at an optional 48 hour time point after LUM015 injection and subjects returned to the study site once a week for 2 weeks after surgery for evaluations consisting of vital signs, laboratory studies, and documentation of any APA. PFTs were repeated at the 2 week visit. An end of study assessment occurred 30-35 days post LUM015 administration for APA. Patient blood samples were collected before and in the 24-48 hours after LUM015 administration for pharmacokinetic and pharmacodynamic studies.

Patients underwent standard operative and peri-operative treatment. Resected patient tissues underwent standard surgical pathology procedures before being imaged and sampled for the study with the guidance of a clinical pathologist blinded to the fluorescence imaging measurements.

Mouse Study Design

All animal studies were performed in accordance with protocols approved by the Duke University or Massachusetts General Hospital (MGH) Institutional Animal Care and Use Committee. The objective of the controlled laboratory experiments was to use a primary mouse model of soft tissue sarcoma and orthotopic models of breast cancer to explore the mechanism of LUM015 distribution and activation *in vivo*. We used genetically engineered mice to model the *in vivo* activity of LUM015 as well as a source for tissues and cell lines for *in vitro* studies. Sample sizes were selected prior to initiating the study based on prior intraoperative imaging studies conducted in the lab (*16*) and power calculations performed as described previously (*36*).

Data collection was stopped if a smaller sample size achieved statistical significance. No outliers were excluded in this study. The mice in this study were not randomized to their treatments and were selected based on availability. The investigators were not blinded when performing tissue fluorescence measurements. Histological examination was performed by a pathologist blinded to the fluorescence imaging measurements.

Tumor-bearing mice

Primary soft tissue sarcomas were generated using the previously described alleles, *LSL-Kras^{G12D}(37), Braf^{CA}(38), p53^{Fl}* (*39*), and *LSL-YFP(40)*. *LSL-YFP* mice were obtained from Jackson Laboratory (Bar Harbor, ME). STS were initiated by intramuscular injection of an adenovirus expressing Cre-recombinase as previously described (*41*) into the hind limb or mice with the genotype *Braf$^{CA/+}$;p53$^{fl/fl}$* (*BP*) or *LSL-YFP; LSL-Kras$^{G12D/+}$; p53$^{fl/fl}$* (*KPY*). *BP* mice were used for all experiments except flow cytometry studies, where *KPY* mice were used. Mice were administered LUM015 or LUM033 via tail vein injection when tumors reached about 1000 mm^3. After a specified time interval, the animals were euthanized and tumor and normal tissues were removed for fluorescence imaging and other analyses. Alternatively, tumors were removed and intraoperative assessment of residual fluorescence was performed as described previously (*16*), and animals were monitored for local recurrence. After tumor resection, *in vivo* imaging of the tumor bed was performed with the LUM imaging device to test for the presence of residual fluorescence followed by closure of the surgical wound. Blood samples for pharmacokinetic studies were obtained from the submandibular vein.

Orthotopic breast cancers were generated using MMTV-PyVT, FVB and BALB/c mice originally obtained from Jackson Laboratories and bred and maintained in the Cox-7 gnotobiotic animal facility of Edwin L. Steele Laboratory at MGH. Spontaneous tumors were excised when

they reached ~8mm in diameter and a ~1 mm^3 piece of viable tumor tissue was transplanted orthotopically into syngeneic FVB female mice (*42*). Alternatively, single breast tumors were established by implanting 1 x 10^5 4T1 cells into the third mammary fat pad (*43*). 4T1 cells (ATCC) were cultured in high-glucose DMEM (ATCC) with 10% FBS and 1% MEM NEAA (Invitrogen). Cell lines were authenticated in 2013 by IDEXX laboratories (IDEXX RADIL Case #14116-2013) and to found to be identical to the profile established for the 4T1 cell line (ATCC #CRL-2539). When tumors reached 4-5 mm in diameter, administration of LUM015, imaging, and other analyses were performed as described above.

Fluorescence Imaging

The handheld LUM imaging device was described previously (*16*). Excitation illumination from a 300-Watt Xenon lamp (Sunoptic Technologies, Jacksonville, Florida) was collimated and reflected toward a 627.5-672.5 nm band-pass excitation filter and then reflected toward the specimen. The fluorescence emission was filtered by a 685-735 nm band pass element and relayed onto a charge coupled device (CCD) (PixelFly QE; PCO AG, Kelheim, Germany) which was connected to a computer for image acquisition and display. Normal and tumor tissues were identified grossly and the imaging tip was applied to the tissue to obtain 2-3 images of the same location. The tissue was biopsied at the site of imaging for identification of the tissue type by histological analysis and measurement of LUM015 metabolites.

Image Analysis

Image processing was performed using a custom script developed in the Matlab programming environment (MathWorks, Natick, MA). This script applied standard corrections for background and signal distribution (*44*). A dark field background image was subtracted from both the image under study and a flat field correction image in order to eliminate background signal. The image

under study was then divided by the background-corrected flat-field image to correct for signal variations across the field of view. A 6 mm diameter cropping mask centered on the two dimensional CCD array was applied to the image under study prior to the generation of image statistics. Mean pixel intensities derived from the Matlab script are reported in this study.

For visual representation of images, the contrast and brightness of images were adjusted as described previously (*16*) so that the reader can appreciate the differences in fluorescence intensities between tumor and normal tissue. Brightness and contrast settings were determined based on the tumor image histogram and then applied to all images from the same patient or mouse.

Histological Analysis

Sample tissues were formalin fixed, paraffin embedded and sectioned to create 5 micron thick Hematoxylin and Eosin (H&E) stained slides. Slides were reviewed with a clinical pathologist specializing in STS (DMC) who was blinded to tissue fluorescence measurements.

Immunohistochemistry and Immunofluorescence

Formalin fixed, paraffin embedded tissue samples from mice and humans injected with LUM015 were obtained. 5 μm thick unstained sections were deparaffinized with xylene and rehydrated with a grades series of ethanol and water washes before immunostaining. For PEG immunohistochemistry and immunofluorescence studies, the primary antibody was rat anti-PEG used at concentrations of 1:175 and 1:200, respectively (Abcam). For immunohistochemistry, the secondary antibody was biotinylated rabbit anti-rat immunoglobulin G (1:200, Vector) and eight 40X fields were scored for intensity of PEG staining according to the following scale: 0- no staining, 1- minimal staining, 2- moderate staining, 3- intense staining. Scoring was done by

three independent researchers who were blinded to the identity of the sample and the average score was used, rounded to the nearest whole number. For immunofluorescence, the secondary antibody was Alexa Fluor 488-conjugated goat anti-rat immunoglobulin M (1:200, Life Technologies). Nuclear staining was performed using Hoechst 33342 dye (1:1000, Life Technologies). Pictures were acquired with a Leica SP5 inverted confocal microscope (Leica Microsystems) using Leica Suite software (Leica microsystems).

Flow Cytometry

KPY mice harboring primary sarcomas were injected with either 3.5 mg/kg of LUM015 or PBS vehicle and tumors were collected 6 hours after injection. Cells were dissociated from tumors according to methods described previously (*45*). Total cells dissociated from tumors were incubated with rat anti-mouse CD16/32 IgG (BD Pharmigen) and phycoerythrin (PE)-Cy5 conjugated anti-mouse CD11b IgG (eBioscience). Data were collected from at least 200,000 cells by FACSCanto (BD Pharmigen) an analyzed by Flowjo (Tree Star, Inc).

Liquid Chromatography/Mass spectrometry

To prepare plasma samples, 20 µl of plasma was incubated at 45º C for 4 hours in a 2 mL polypropylene screw-cap vial with 8 µl of 1 ug/mL Fragment 1-$^{13}C_{10}{}^{15}N_6$ (internal standard) and 20 µl of 2.5 mg/mL trypsin in PBS. After cooling to room temperature, 100 µl of 2% formic acid in acetonitrile was added to precipitate proteins followed by centrifugation for 5 minutes at 16,000 g and removal of 20 µl of the supernatant for liquid chromatography/mass spectrometry (LC/MS/MS). For tissue measurements, 50 µl of sample containing 1 part tissue homogenate and 2 parts H_20 was incubated with 10 µl of 1 µg/mL Fragment 1-$^{13}C_{10}{}^{15}N_6$ (internal standard) and 25 mg/mL trypsin in PBS. Following protein precipitation and centrifugation, 10 µl of the supernatant was used for LC/MS/MS analysis. Calibration samples were prepared by adding

known amounts of pure Fragment 1 or LUM015 to control plasma or tissue homogenate and processed as above.

A Shimadzu 20A series liquid chromatography system with binary pumps, an autosampler, and column oven was used. We used a 4.6 x 50 mm C18 Phenomenex Kinetex column with a 4 x 3 mm Kinetex guard column at 45ºC. Samples were kept at 4ºC. Mobile phase A: 0.1% formic acid in 80:20 water:acetonitrile. Mobile phase B: acetonitrile. A 1 mL/min flow rate was used with the following elution gradient: 20-95% B for 0-1 min, 95% B for 1-2.5 min, 95-20% B for 2.5-2.6 min, and 20% B for 2.6-4 min for equilibration. Total run time was 5 minutes.

For electrospray ionization mass spectrometry (ESI-MS/MS) an AB/SCIEX API 4000 QTrap tandem-mass spectrometer was used. Optimization of parameters for positive mode electrospray (declustering potential, temperature, gas flow) and mass spectrometer (parent/daughter ions, quadrupole potential) was performed by direction infusion of the pure analyte Fragment 1 in to the ESI-LC/MS/MS system. The following multiple reaction monitoring (MRM) transitions were monitored for quantification (m/z units): Fragment 1 parent ion $(M+H)^{2+}$/daughter ion fragment as 533.2/371 and Fragment 1-$^{13}C_{10}{}^{15}N_6$ parent ion $(M+H)^{2+}$/daughter ion fragment as 541.1/371. Analysis of calibration samples in the range of 7.0-870 nM for plasma and 3.5-870 nM for tissue showed a linear response (r=0.999 criterion) and the low limits of quantification (LLOQ) were confirmed as 7 nM for plasma and 3.5 nM for tissue at a +/- 80% accuracy criterion.

High Pressure Liquid Chromatography coupled with Absorbance and Fluorescence Detection

To prepare samples, 30 µl of plasma or tissue homogenate (1 part tissue + 2 parts H_20) was shaken vigorously for 20 seconds at speed 4 in a FastPrep apparatus (Thermo-Savant) with 60 µl

methanol and 10 glass beads (1 mm, Bio Spec Inc.) in a 200 µl polypropylene conical vial. The supernatant was added to 30 µl of 0.1% formic acid in water and 50 µl was injected into the high pressure liquid chromatography (HPLC) system.

For HPLC, a Waters 2695 pump/autosampler/ column heater module was used with a 3 x 250 mm Phenomenex Hydro-RP column and 4 x 3 mm Kinetex guard column at 50º C. Samples were kept at 10º C. Mobile phase A consisted of 0.1% formic acid in water and mobile phase B was methanol. The flow rate was 0.7 mL/min and the elution gradient was as follows: 10-30% B for 0-2 min, 30-90% B for 2-12 min, 90% B for 12-16 min, 90-10% B for 16-17 min, and 10% B for 17-27 min as equilibration. The total run time was 27 minutes.

We used a Waters 2475 fluorescence detector (FD) with excitation at 649 nm and emission at 670 nm and a gain of 10 along with a Waters 2487 UV/Vis absorbance detector at 649 nm. The solvent flow from the column was split and adjusted to be equal (0.35 mL/min to each detector) to provide for equal peak retention time on both fluorescence and absorption chromatograms, allowing for Fragment 2 identification. Separate sets of calibration samples in the 0.0375-300 µM range were prepared for LUM015, Fragment 2, and Fragment 3 by adding pure standards to control tumor homogenates. Linear calibration responses were obtained for all three analytes in the concentration range measured (r=0.999 criterion) and the LLOQs were confirmed to be 37.5 nM at +/- 80% accuracy criterion.

Statistics

Results are presented as means +/- standard error of the mean (SEM) unless otherwise indicated. Two-tailed student's *t* test was performed to compare the means of two groups and a matched pair *t* test was used when comparing fluorescent measurements from the same patient. A Mann-Whitney test was performed to compare the means of two groups when data was distributed non-

parametrically. Two-way ANOVA was performed to examine the interaction between two independent variables such as dose and imaging time and one-way ANOVA was used when measuring the effect of only one variable, such as tissue type. These were followed by Bonferroni or Tukey's post hoc multiple comparison tests for pairwise comparisons of individual treatments or tissue types. For local recurrence studies, Kaplan-Meir analysis was performed with the log-rank test for statistical significance. To find the correlation of two different measurements from the same sample, we determined the Pearson coefficient (r) and r^2. Significance was assumed at $P<0.05$. All calculations were performed using Prism 6 (GraphPad).

Supplementary Materials:

Figure S1. *In vitro* protease activation of LUM015.

Figure S2. LUM015 fluorescently labels tumors in a mouse model of breast cancer.

Figure S3. The percentage of tumor cells that are Cy5+ after administration of LUM015.

Figure S4. *In vivo* detection of residual fluorescence within the tumor bed.

Table S1. Additional patient data from the first-in-human Phase I clinical trial of LUM015.

Table S2. Summary pharmacokinetic data from mice and humans.

Table S3. *Ex vivo* Imaging.

Figure S5. *In vitro* incubation of LUM015 with mouse tissues.

Table S5. Correlating tissue fluorescence with metabolite concentration.

Figure S6. Increased distribution of LUM015 to tumor tissues correlates with tumor-selective fluorescence.

References:

1. J. C. Yang, A. E. Chang, A. R. Baker, W. F. Sindelar, D. N. Danforth, S. L. Topalian, T. DeLaney, E. Glatstein, S. M. Steinberg, M. J. Merino, S. A. Rosenberg, Randomized prospective study of the benefit of adjuvant radiation therapy in the treatment of soft tissue sarcomas of the extremity. *Journal of clinical oncology : official journal of the American Society of Clinical Oncology* **16**, 197-203 (1998).
2. P. W. Pisters, D. H. Leung, J. Woodruff, W. Shi, M. F. Brennan, Analysis of prognostic factors in 1,041 patients with localized soft tissue sarcomas of the extremities. *Journal of clinical oncology : official journal of the American Society of Clinical Oncology* **14**, 1679-1689 (1996).
3. B. Fisher, S. Anderson, J. Bryant, R. G. Margolese, M. Deutsch, E. R. Fisher, J. H. Jeong, N. Wolmark, Twenty-year follow-up of a randomized trial comparing total mastectomy, lumpectomy, and lumpectomy plus irradiation for the treatment of invasive breast cancer. *The New England journal of medicine* **347**, 1233-1241 (2002).
4. J. D. Beane, J. C. Yang, D. White, S. M. Steinberg, S. A. Rosenberg, U. Rudloff, Efficacy of adjuvant radiation therapy in the treatment of soft tissue sarcoma of the extremity: 20-year follow-up of a randomized prospective trial. *Annals of surgical oncology* **21**, 2484-2489 (2014).
5. D. Wang, Q. Zhang, B. L. Eisenberg, J. M. Kane, X. A. Li, D. Lucas, I. A. Petersen, T. F. DeLaney, C. R. Freeman, S. E. Finkelstein, Y. J. Hitchcock, M. Bedi, A. K. Singh, G. Dundas, D. G. Kirsch, Significant Reduction of Late Toxicities in Patients With Extremity Sarcoma Treated With Image-Guided Radiation Therapy to a Reduced Target Volume: Results of Radiation Therapy Oncology Group RTOG-0630 Trial. *Journal of clinical oncology : official journal of the American Society of Clinical Oncology*, (2015).
6. M. S. Anscher, P. Jones, L. R. Prosnitz, W. Blackstock, M. Hebert, R. Reddick, A. Tucker, R. Dodge, G. Leight, Jr., J. D. Iglehart, et al., Local failure and margin status in early-stage breast carcinoma treated with conservation surgery and radiation therapy. *Annals of surgery* **218**, 22-28 (1993).
7. J. C. Cendan, D. Coco, E. M. Copeland, 3rd, Accuracy of intraoperative frozen-section analysis of breast cancer lumpectomy-bed margins. *Journal of the American College of Surgeons* **201**, 194-198 (2005).
8. Q. R. Tummers, F. P. Verbeek, B. E. Schaafsma, M. C. Boonstra, J. R. van der Vorst, G. J. Liefers, C. J. van de Velde, J. V. Frangioni, A. L. Vahrmeijer, Real-time intraoperative detection of breast cancer using near-infrared fluorescence imaging and Methylene Blue. *European journal of surgical oncology : the journal of the European Society of Surgical Oncology and the British Association of Surgical Oncology* **40**, 850-858 (2014).
9. N. Kosaka, M. Mitsunaga, M. R. Longmire, P. L. Choyke, H. Kobayashi, Near infrared fluorescence-guided real-time endoscopic detection of peritoneal ovarian cancer nodules using intravenously injected indocyanine green. *International journal of cancer. Journal international du cancer* **129**, 1671-1677 (2011).
10. R. Weissleder, Molecular imaging in cancer. *Science* **312**, 1168-1171 (2006).
11. G. M. van Dam, G. Themelis, L. M. Crane, N. J. Harlaar, R. G. Pleijhuis, W. Kelder, A. Sarantopoulos, J. S. de Jong, H. J. Arts, A. G. van der Zee, J. Bart, P. S. Low, V. Ntziachristos, Intraoperative tumor-specific fluorescence imaging in ovarian cancer by folate receptor-alpha targeting: first in-human results. *Nature medicine* **17**, 1315-1319 (2011).
12. Y. Ardeshirpour, M. Hassan, R. Zielinski, J. Horton, J. Capala, A. H. Gandjbakhche, V. Chernomordik, In vivo assessment of HER2 receptor density in HER2-positive tumors by near-infrared imaging, using repeated injections of the fluorescent probe. *Technology in cancer research & treatment* **13**, 427-434 (2014).

13. R. Weissleder, C. H. Tung, U. Mahmood, A. Bogdanov, Jr., In vivo imaging of tumors with protease-activated near-infrared fluorescent probes. *Nature biotechnology* **17**, 375-378 (1999).
14. J. E. Koblinski, M. Ahram, B. F. Sloane, Unraveling the role of proteases in cancer. *Clinica chimica acta; international journal of clinical chemistry* **291**, 113-135 (2000).
15. M. M. Mohamed, B. F. Sloane, Cysteine cathepsins: multifunctional enzymes in cancer. *Nature reviews. Cancer* **6**, 764-775 (2006).
16. J. K. Mito, J. M. Ferrer, B. E. Brigman, C. L. Lee, R. D. Dodd, W. C. Eward, L. F. Marshall, K. C. Cuneo, J. E. Carter, S. Ramasunder, Y. Kim, W. D. Lee, L. G. Griffith, M. G. Bawendi, D. G. Kirsch, Intraoperative detection and removal of microscopic residual sarcoma using wide-field imaging. *Cancer* **118**, 5320-5330 (2012).
17. S. Bartholf DeWitt, C. Eward, W. C. Eward, A. L. Lazarides, D. G. Kirsch, D. M. Cardona, B. E. Brigman, J. K. Mito, M. J. Whitley, J. M. Ferrer, D. B. Strasfeld, D. Lee, K. Concannon, G. Spodnick, E. Holmes, K. Miller, J. Berg, in *The American College of Veterinary Surgeons 2014 Surgery Summitt*. (San Diego, California, 2014).
18. E. J. Freireich, E. A. Gehan, D. P. Rall, L. H. Schmidt, H. E. Skipper, Quantitative comparison of toxicity of anticancer agents in mouse, rat, hamster, dog, monkey, and man. *Cancer Chemother Rep* **50**, 219-244 (1966).
19. K. C. Cuneo, J. K. Mito, M. P. Javid, J. M. Ferrer, Y. Kim, W. D. Lee, M. G. Bawendi, B. E. Brigman, D. G. Kirsch, Imaging primary mouse sarcomas after radiation therapy using cathepsin-activatable fluorescent imaging agents. *International journal of radiation oncology, biology, physics* **86**, 136-142 (2013).
20. B. O'Sullivan, A. M. Davis, R. Turcotte, R. Bell, C. Catton, P. Chabot, J. Wunder, R. Kandel, K. Goddard, A. Sadura, J. Pater, B. Zee, Preoperative versus postoperative radiotherapy in soft-tissue sarcoma of the limbs: a randomised trial. *Lancet* **359**, 2235-2241 (2002).
21. K. L. Linegar, A. E. Adeniran, A. F. Kostko, M. A. Anisimov, Hydrodynamic Radius of Polyethylene Glycol in Solution Obtained by Dynamic Light Scattering. *Colloid Journal* **72**, 3 (2010).
22. E. Segal, T. R. Prestwood, W. A. van der Linden, Y. Carmi, N. Bhattacharya, N. Withana, M. Verdoes, A. Habtezion, E. G. Engleman, M. Bogyo, Detection of intestinal cancer by local, topical application of a quenched fluorescence probe for cysteine cathepsins. *Chemistry & biology* **22**, 148-158 (2015).
23. C. Bremer, C. H. Tung, R. Weissleder, In vivo molecular target assessment of matrix metalloproteinase inhibition. *Nature medicine* **7**, 743-748 (2001).
24. E. S. Olson, T. Jiang, T. A. Aguilera, Q. T. Nguyen, L. G. Ellies, M. Scadeng, R. Y. Tsien, Activatable cell penetrating peptides linked to nanoparticles as dual probes for in vivo fluorescence and MR imaging of proteases. *Proceedings of the National Academy of Sciences of the United States of America* **107**, 4311-4316 (2010).
25. C. Bremer, V. Ntziachristos, B. Weitkamp, G. Theilmeier, W. Heindel, R. Weissleder, Optical imaging of spontaneous breast tumors using protease sensing 'Smart' optical probes. *Invest Radiol* **40**, 321-327 (2005).
26. A. G. Terwisscha van Scheltinga, G. M. van Dam, W. B. Nagengast, V. Ntziachristos, H. Hollema, J. L. Herek, C. P. Schroder, J. G. Kosterink, M. N. Lub-de Hoog, E. G. de Vries, Intraoperative near-infrared fluorescence tumor imaging with vascular endothelial growth factor and human epidermal growth factor receptor 2 targeting antibodies. *Journal of nuclear medicine : official publication, Society of Nuclear Medicine* **52**, 1778-1785 (2011).
27. T. Quillard, K. Croce, F. A. Jaffer, R. Weissleder, P. Libby, Molecular imaging of macrophage protease activity in cardiovascular inflammation in vivo. *Thrombosis and haemostasis* **105**, 828-836 (2011).

28. C. E. Lewis, J. W. Pollard, Distinct role of macrophages in different tumor microenvironments. *Cancer research* **66**, 605-612 (2006).
29. E. Y. Lin, A. V. Nguyen, R. G. Russell, J. W. Pollard, Colony-stimulating factor 1 promotes progression of mammary tumors to malignancy. *The Journal of experimental medicine* **193**, 727-740 (2001).
30. G. W. Caldwell, J. A. Masucci, Z. Yan, W. Hageman, Allometric scaling of pharmacokinetic parameters in drug discovery: can human CL, Vss and t1/2 be predicted from in-vivo rat data? *European journal of drug metabolism and pharmacokinetics* **29**, 133-143 (2004).
31. T. Kolokotrones, S. Van, E. J. Deeds, W. Fontana, Curvature in metabolic scaling. *Nature* **464**, 753-756 (2010).
32. W. P. Caron, H. Clewell, R. Dedrick, R. K. Ramanathan, W. L. Davis, N. Yu, M. Tonda, J. H. Schellens, J. H. Beijnen, W. C. Zamboni, Allometric scaling of pegylated liposomal anticancer drugs. *Journal of pharmacokinetics and pharmacodynamics* **38**, 653-669 (2011).
33. D. N. Gosalia, C. M. Salisbury, J. A. Ellman, S. L. Diamond, High throughput substrate specificity profiling of serine and cysteine proteases using solution-phase fluorogenic peptide microarrays. *Molecular & cellular proteomics : MCP* **4**, 626-636 (2005).
34. G. M. Thurber, R. Weissleder, A systems approach for tumor pharmacokinetics. *PloS one* **6**, e24696 (2011).
35. N. Bertrand, J. Wu, X. Xu, N. Kamaly, O. C. Farokhzad, Cancer nanotechnology: the impact of passive and active targeting in the era of modern cancer biology. *Advanced drug delivery reviews* **66**, 2-25 (2014).
36. W. D. Dupont, W. D. Plummer, Jr., Power and sample size calculations. A review and computer program. *Controlled clinical trials* **11**, 116-128 (1990).
37. E. L. Jackson, N. Willis, K. Mercer, R. T. Bronson, D. Crowley, R. Montoya, T. Jacks, D. A. Tuveson, Analysis of lung tumor initiation and progression using conditional expression of oncogenic K-ras. *Genes & development* **15**, 3243-3248 (2001).
38. D. Dankort, E. Filenova, M. Collado, M. Serrano, K. Jones, M. McMahon, A new mouse model to explore the initiation, progression, and therapy of BRAFV600E-induced lung tumors. *Genes & development* **21**, 379-384 (2007).
39. J. Jonkers, R. Meuwissen, H. van der Gulden, H. Peterse, M. van der Valk, A. Berns, Synergistic tumor suppressor activity of BRCA2 and p53 in a conditional mouse model for breast cancer. *Nature genetics* **29**, 418-425 (2001).
40. S. Srinivas, T. Watanabe, C. S. Lin, C. M. William, Y. Tanabe, T. M. Jessell, F. Costantini, Cre reporter strains produced by targeted insertion of EYFP and ECFP into the ROSA26 locus. *BMC developmental biology* **1**, 4 (2001).
41. D. G. Kirsch, D. M. Dinulescu, J. B. Miller, J. Grimm, P. M. Santiago, N. P. Young, G. P. Nielsen, B. J. Quade, C. J. Chaber, C. P. Schultz, O. Takeuchi, R. T. Bronson, D. Crowley, S. J. Korsmeyer, S. S. Yoon, F. J. Hornicek, R. Weissleder, T. Jacks, A spatially and temporally restricted mouse model of soft tissue sarcoma. *Nature medicine* **13**, 992-997 (2007).
42. Y. Huang, J. Yuan, E. Righi, W. S. Kamoun, M. Ancukiewicz, J. Nezivar, M. Santosuosso, J. D. Martin, M. R. Martin, F. Vianello, P. Leblanc, L. L. Munn, P. Huang, D. G. Duda, D. Fukumura, R. K. Jain, M. C. Poznansky, Vascular normalizing doses of antiangiogenic treatment reprogram the immunosuppressive tumor microenvironment and enhance immunotherapy. *Proceedings of the National Academy of Sciences of the United States of America* **109**, 17561-17566 (2012).
43. E. I. Ager, S. V. Kozin, N. D. Kirkpatrick, G. Seano, D. P. Kodack, V. Askoxylakis, Y. Huang, S. Goel, M. Snuderl, A. Muzikansky, D. M. Finkelstein, D. T. Dransfield, L. Devy, Y. Boucher, D. Fukumura, R. K. Jain, Blockade of MMP14 Activity in Murine Breast Carcinomas: Implications for Macrophages, Vessels, and Radiotherapy. *Journal of the National Cancer Institute* **107**, (2015).

44. in *Methods in cell biology,* D. P. Taylor, Y. Wang, L. Wilson, Eds. (1989), vol. 29, pp. 1-328.
45. M. Sachdeva, J. K. Mito, C. L. Lee, M. Zhang, Z. Li, R. D. Dodd, D. Cason, L. Luo, Y. Ma, D. Van Mater, R. Gladdy, D. C. Lev, D. M. Cardona, D. G. Kirsch, MicroRNA-182 drives metastasis of primary sarcomas by targeting multiple genes. *The Journal of clinical investigation* **124**, 4305-4319 (2014).

Acknowledgments:

We thank Yan Ma, Nerissa Williams, and Lixia Luo for valuable assistance with histology, animal/human tissue imaging, and mouse colony management, respectively. We thank Julia Kahn for her technical assistance with the mice in the breast cancer studies. We thank Patrick O'Donnell, MD PhD of the University of Kentucky, Francis Hornicek, MD PhD of the Massachusetts General Hospital, Sam Yoon, MD of the Memorial Sloan Kettering Cancer Center, and Robert Noveck, MD PhD of Duke University for serving on the patient safety committee for the Phase I study. **Funding**: The work was supported in part by an ASCO Advanced Clinical Research Award (DGK), NIH T32 grant #T32GM007171 (MJW, JKM), NCI Small Business Innovation Research award #1U43CA165024 (WDL), National Center for Advancing Translational Science of the NIH Grant #UL1TR001117 (EKO) and by Duke Comprehensive Cancer Center Support Grant 5P30-CA-014236-38. **Author contributions**: MJW participated in the design and execution of the clinical protocol, designed and performed experiments, analyzed and interpreted data, and wrote the manuscript. DMC analyzed and interpreted data. ALL, IS and CLL designed and performed experiments, analyzed and interpreted data, and contributed to the manuscript. MS designed and performed experiments and analyzed and interpreted data. JMF, DBS, WDL, LGG, and MGB participated in the design of the clinical protocol, designed experiments, and analyzed and interpreted data. JC participated in the design of the clinical protocol, identified human subjects and participated in sample

procurement. DGB, SEW, RAG, and PJM identified human subjects and participated in sample procurement. JKM designed and performed experiments, analyzed and interpreted data, and edited the manuscript. KCC, NAL, EKO, RFR, and WCE participated in the design of the clinical protocol and edited the manuscript. EKO drafted, submitted, and maintained the IND related to the Phase I study. DF and RJK analyzed and interpreted data and contributed to the manuscript. RFR and BEB served on the safety monitoring committee. DGK participated in the design of the clinical protocol, held the IND, designed and oversaw the laboratory studies, interpreted the data, and wrote the manuscript. BEB designed and supervised the clinical protocol, participated in sample procurement, and edited the manuscript. **Competing interests**: WDL is a cofounder and CEO of Lumicell, Inc., a company that is attempting to commercialize LUM015 and the LUM imaging system. MGB is a cofounder of Lumicell, Inc. and is a member of its scientific advisory board. LGG and DGK are members of the Lumicell, Inc. scientific advisory board. JMF and DBS are employees of Lumicell, Inc. WDL, MGB, and JMF are co-inventors of LUM015 under U.S. patent application 20140301950. WDL, MGB, JMF, and DGK are co-inventors of the hand-held imaging device under US patent application 2009299196.

Clinical Trial: The Phase I clinical trial is registered with www.clinicaltrials.gov (NCT01626066).

Figures:

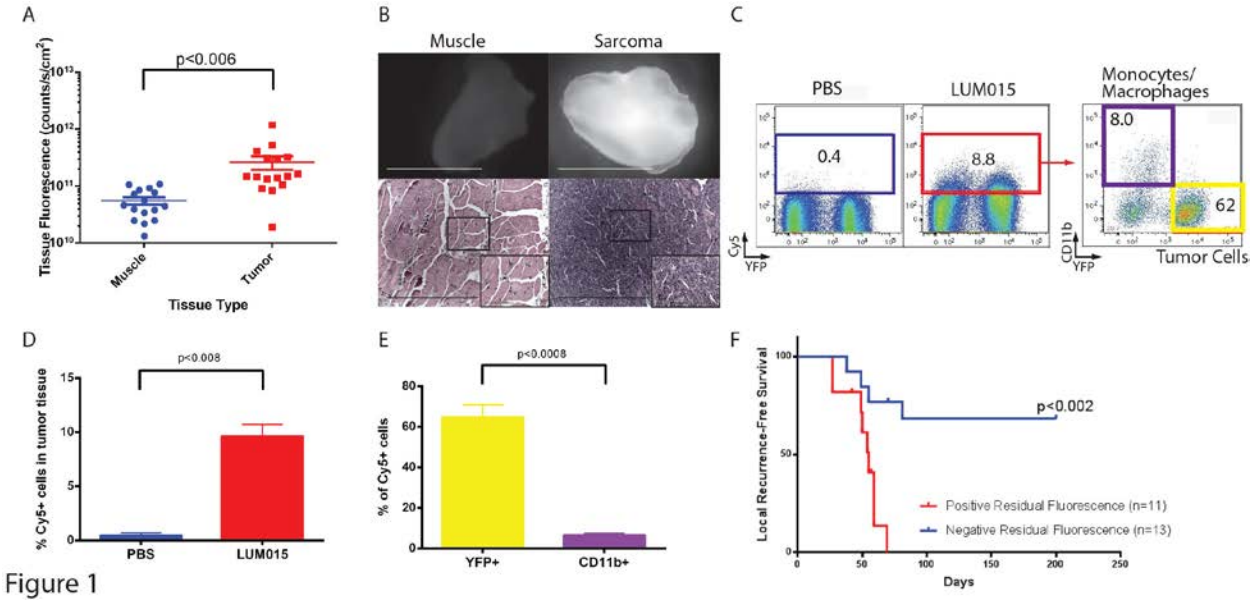

Figure 1

Figure 1: LUM015 fluorescently labels tumor cells in a primary mouse model of STS. Mice with primary STS were administered intravenous LUM015 with subsequent imaging of tissues using the LUM device. **(A)** The mean measured fluorescence was significantly higher in tumor when compared to the mean fluorescence from muscle ($p<0.006$, unpaired *t*-test, n=16 mice, $mean_{muscle}=5.6 \times 10^{10}$ counts/s/cm^2, $mean_{tumor}= 2.7 \times 10^{11}$ counts/s/cm^2). **(B)** Representative fluorescence images of resected normal muscle (left) and sarcoma (right) are shown along with corresponding hematoxylin and eosin (H&E) stained histology below (scale bars = 5 mm for fluorescence images, 500 µm for H&E images, and 100 µm for high magnification insets). The same contrast scale was applied to both fluorescence images. **(C)** Representative flow cytometry analysis of resected mouse tumors expressing a tumor cell-specific YFP marker after intravenous administration of PBS or a 3.5 mg/kg dose of LUM015. Note the tumor injected with LUM015 has as an increase in the percentage of Cy5+ cells (red box), which are mostly YFP+ tumor cells (yellow box). **(D,E)** Quantification of flow cytometry data showing that **(D)** LUM015 injected

mice have a significant increase in the percentage of Cy5+ cells in the tumor ($p<0.008$, unpaired *t*-test, $n_{PBS}=2$ mice, $n_{LUM015}= 3$ mice**)** and that **(E)** these fluorescent cells are mostly YFP+ tumor cells with some CD11b+ tumor associated macrophages ($p<0.0008$, unpaired *t*-test, n=3 mice), respectively. (**F**) In a mouse model of tumor resection, residual fluorescence within the tumor bed measured before wound closure predicted local recurrence ($p<0.002$, Log-rank test). Error bars represent SEM.

Patient #	LUM015 Dose (mg/kg)	Imaging Time (Hr)	Tumor Type	Tumor Grade	Tumor Size (cm)	Neoadjuvant Therapy	Tumor Site
1	0.5	30.1	Well-differentiated Liposarcoma	Low	10.5 x 8.5 x 6.2	None	Retroperitoneal
2	0.5	28.5	UPS	High	13.5 x 8.3 x 6.5	25 x 2 Gy RT	Thigh
3	0.5	28.5	UPS	High	18.0 x 9.0 x 6.0	25 x 2 Gy RT	Upper Arm
4	1	30.9	Malignant Peripheral Nerve Sheath Tumor	Intermediate	2.5 x 1.6 x 1.5	25 x 2 Gy RT	Upper Arm
5	1	26.9	Myxoinflammatory fibroblastic sarcoma/ hemosiderotic fibrolipomatous tumor	Low	31.0 x 20.0 x 1.3	None	Leg
6	1	26.5	UPS	High	3.6 x 2.9 x. 1.2	None	Upper Arm
7	1	4.8	Metastatic Clear Cell Sarcoma	High	4.0 x 2.9 x 2.8	None	Inguinal Lymph Node
8	1	7.2	UPS	High	13.0 x 6.5 x 7.1	25 x 2 Gy RT	Upper Arm
9	1	8.3	IDC: ER+, PR-, Her2+	High	3.7	None	Breast
10	1.5	9.6	IDC: ER+, PR+, Her2-	Intermediate	7.5 x 2.5 x 1.5	None	Breast
11	1.5	5.1	Metastatic Spindle Cell Sarcoma	Low	0.9	None	Thigh
12	1.5	7.3	Myxofibrosarcoma	High	11.0 x 6.5 x 6.5	None	Thigh
13	0.5	9.6	Synovial Sarcoma	High	20.0 x 12.0 x 6.0	25 x 2 Gy RT	Thigh
14	0.5	8.5	Spindle Cell Sarcoma	High	7.5	25 x 2 Gy RT	Thigh
15	0.5	7.3	IDC: ER+, PR+, Her2-	High	2.4 x 1.6 x. 1.4	None	Breast

UPS= Undifferentiated Pleomorphic Sarcoma; IDC= Invasive Ductal Carcinoma
ER= Estrogen Recepter; PR= Progesterone Receptor

Table 1

Table 1: Enrolled patients in first-in-human Phase I clinical trial of LUM015. Fifteen patients were enrolled in the trial at one of three dose cohorts. Imaging time was measured as the number hours elapsed between LUM015 injection and imaging of the resected tissues with the LUM device. Histological descriptors are based on clinical surgical pathology reports.

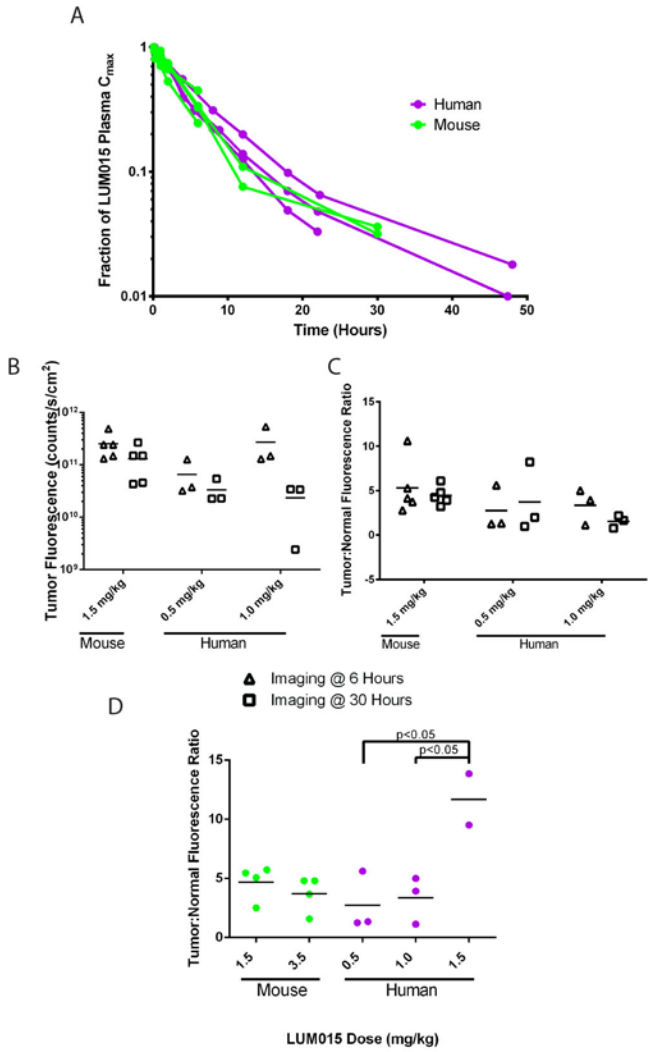

Figure 2

Figure 2: Comparative LUM015 pharmacokinetics in mouse and human subjects. **(A)** The LUM015 plasma clearance profile in mouse and human subjects administered a 1.5 mg/kg dose of LUM015 is similar. Plasma LUM015 concentrations are given as a fraction of the maximum concentration and shown on a log scale. **(B)** In patients, shortening the time between injection of LUM015 and surgery with subsequent tissue imaging from 30 to 6 hours results in increased absolute tumor tissue fluorescence consistent with observations made in mice with primary sarcomas injected with a 1.5 mg/kg dose of LUM015 (Two-way ANOVA, Imaging time effect: $F(1,16)=6.5$, $p<0.03$). **(C)** Similarly, as tumor to normal tissue fluorescence ratios in mice do not

vary significantly with changes in the imaging time, a significant change was not observed upon shortening the imaging time in human subjects (Two-way ANOVA, Imaging time effect: $F(1,16)=0.3$, $p<0.7$). Data in **B**, **C** is from n=5 mice per imaging time and human subjects in the 0.5 mg/kg and 1.0 mg/kg dose cohorts. The 1.5 mg/kg human dose cohort was not included in this analysis because these patients were only imaged at the 6 hour time point. **(D)** Tumor to normal tissue fluorescence ratios measured in human, but not mouse, subjects varied significantly by dose cohort (One-way ANOVA of human data $F(2,5)=9.4$, $p<0.02$; includes all patients imaged at 6 hours except patient ten; $n_{mouse}= 5$ per dose cohort**)**, and the 1.5 mg/kg dose cohort had a significantly higher fluorescence ratio than the two lower dose cohorts (Tukey's multiple comparisons test, $p<0.05$ for 0.5 mg/kg vs 1.5 mg/kg and 1.0 mg/kg vs 1.5 mg/kg).

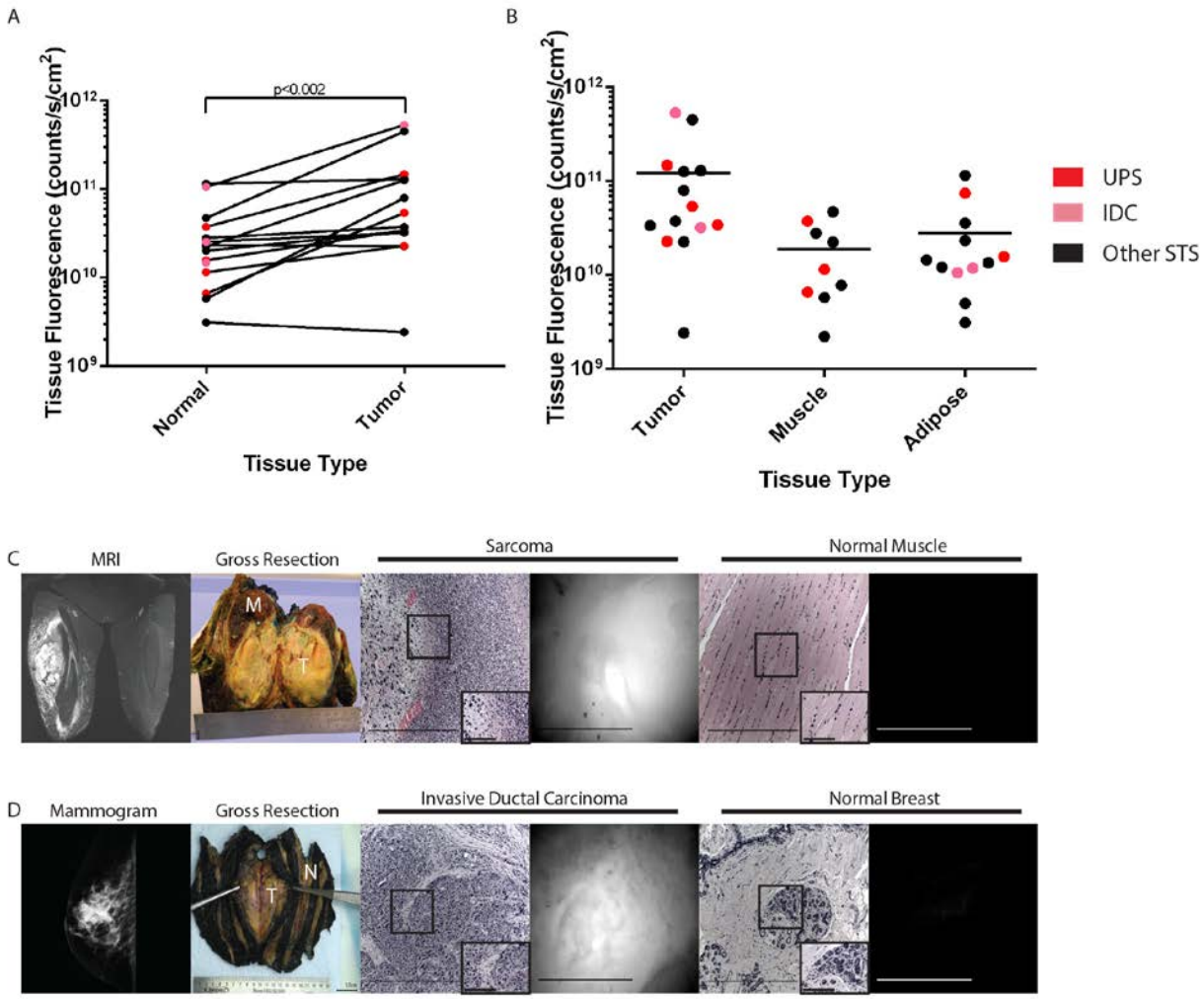

Figure 3

Figure 3: Tumor-selective fluorescence in patients receiving intravenous LUM015 prior to resection. **(A)** Tumor tissue fluorescence is significantly higher than fluorescence measured from adjacent normal tissue in the same patient ($p<0.002$, paired *t*-test, n=14, excludes patient 10). **(B)** The distribution of tumor tissue fluorescence across all patients is significantly different from the distributions of fluorescence values measured in muscle and adipose tissues (one-way ANOVA, $p<0.04$, $n_{tumor}=14$, $n_{muscle}=10$, $n_{adipose}=11$). Data from patients with undifferentiated pleomorphic sarcoma (UPS) shown in red, invasive ductal carcinoma (IDC) of the breast in pink and other STS subtypes in black. Representative human subjects with

undifferentiated pleomorphic sarcoma of the thigh **(C,** patient #2**)** and invasive ductal carcinoma of the breast **(D**, patient #9). **(C)** From left to right, gadolinium-enhanced MRI showing a large UPS of the thigh, gross tissue resection containing tumor (T) and normal muscle (M), H&E staining of imaged tumor tissue, fluorescence image of tumor tissue obtained with LUM device, H&E staining of imaged muscle, fluorescence image of muscle obtained with LUM device. **(D)** From left to right, mammogram of the breast showing invasive ductal carcinoma, gross tissue resection containing tumor (T) and normal breast (N) tissue, H&E staining of tumor, fluorescence image of tumor obtained with LUM device, H&E staining of imaged breast tissue, fluorescence image of breast tissue obtained with LUM device. For each pair of tumor and normal tissue the same contrast scale was applied. Scale bars = 5 mm for fluorescence images, 500 μm for H&E images, and 100 μm for high magnification insets.

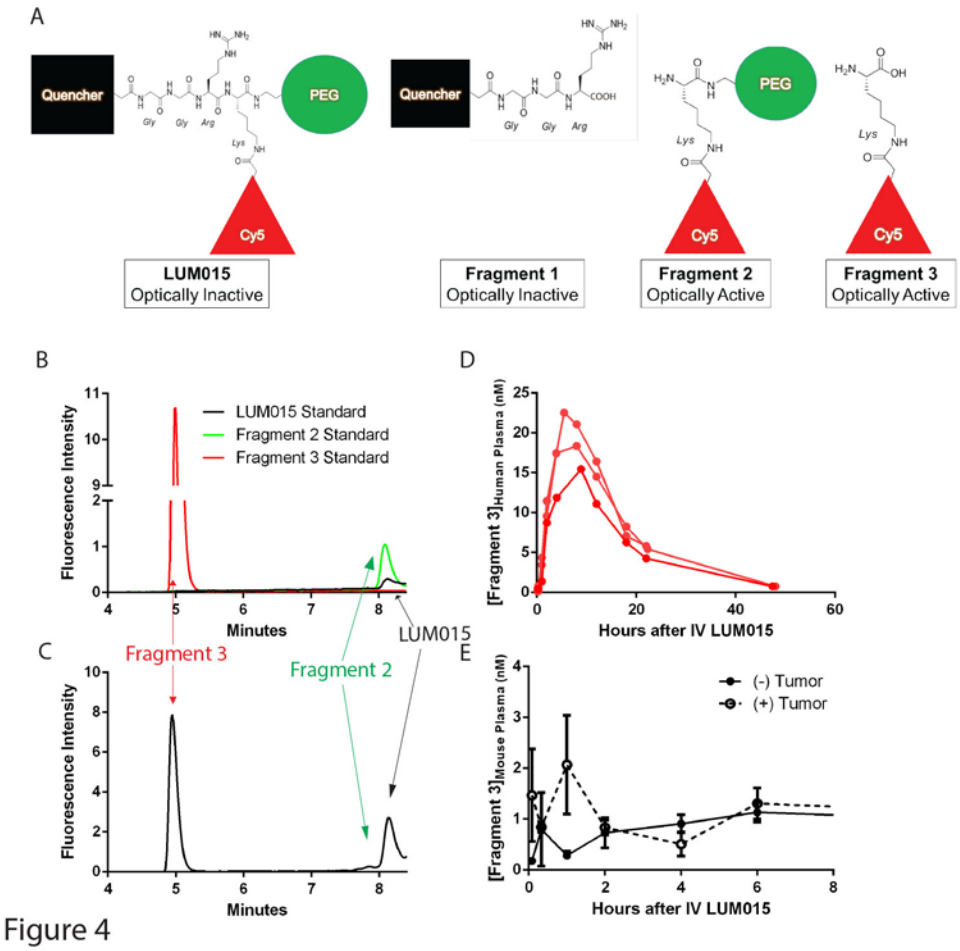

Figure 4

Figure 4: Cy5-Lysine is the major fluorescent LUM015 metabolite. **(A)** Expected LUM015 cleavage products based on the canonical cathepsin protease cleavage site between Arg and Lys, yielding optically inactive Fragment 1 containing the quencher and optically active Fragment 2 containing the Cy5 fluorophore and a 20 kD PEG. Fragment 3 results from cleavage of LUM015 or Fragment 2 in a lysine-promoted manner, yielding a metabolite that contains only a lysine residue with an attached Cy5. **(B)** Analysis of pure LUM015 (25 ng/mL), Fragment 2 (25 ng/mL), and Fragment 3 (2.5 ng/mL) standards using High Pressure Liquid Chromatography coupled with a fluorescence detector (HPLC-FD) showing distinct fluorescent peaks for each metabolite and LUM015 (approximately 1% of Cy5 fluorescence is not absorbed by the quencher). **(C)** HPLC-FD analysis of patient plasma samples revealed Fragment 3 to be the

major metabolite with relatively minimal amounts of Fragment 2. A representative example is shown with plasma collected from patient 14 at 8 hours after intravenous administration of LUM015. **(D)** Human plasma profiles of Fragment 3 in three patients injected with 1.5 mg/kg LUM015 show Fragment 3 levels increasing in the first 8 hours after LUM015 administration with subsequent clearance. **(E)** Tumor-bearing and non-tumor bearing mice were injected with 1.5 mg/kg LUM015 and plasma Fragment 3 concentrations were measured using HPLC-FD , showing that *in vivo* formation of Fragment 3 does not require the presence of tumor cells (error bars represent SEM).

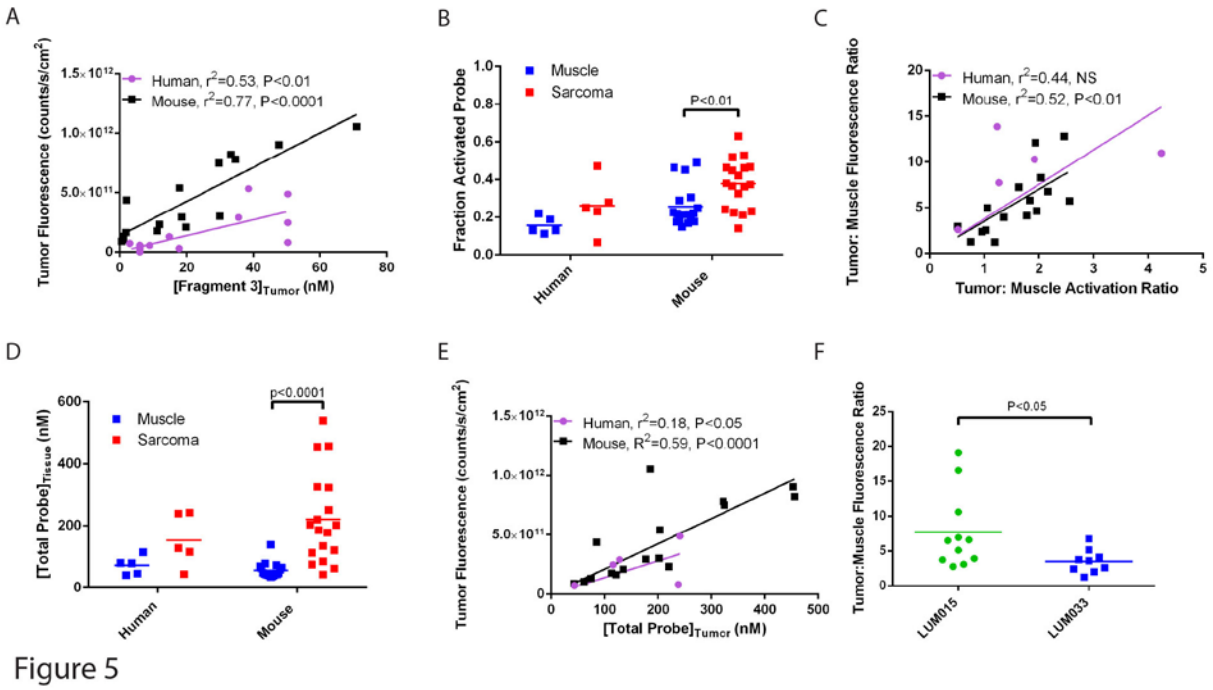

Figure 5

Figure 5: Tumor-selective distribution and activation of LUM015. **(A)** Tissue fluorescence is directly correlated with the concentration of Fragment 3 in mouse and human tumors, measured by HPLC-FD (linear regression with no constraints; Human: r^2=0.53, P<0.01, n=14, data includes 1 tumor sample from each patient except patient 10 where no tumor sample was available; Mouse: r^2=0.77, P<0.0001, n=16, data includes 1 tumor sample from each primary STS-bearing mouse except in two mice where fluorescence was not measured). **(B)** The fraction of activated probe was determined for muscle and tumor tissue samples from human (n=5, patients 8 and 11-14) and mouse (n=18) STS subjects, using the equation: Fraction Activated Probe = ([Fragment 2 (nM)]$_{tissue}$+[Fragment 3 (nM)]$_{tissue}$)/([LUM015 (nM)]$_{tissue}$+[Fragment 2 (nM)]$_{tissue}$+[Fragment 3 (nM)]$_{tissue}$). In both species, the fraction of activated probe was higher in tumors, and this was significant in the mouse cohort (P<0.01, *t*-test). **(C)** There is a strong correlation between the tumor: muscle fluorescence ratio and the Fraction Activated Probe ratio in the mouse cohort (linear regression with y-intercept constrained to the origin, r^2=0.52, P<0.01,

n=16). A comparable correlation is found in the human STS cohort but it is not significant (linear regression with y-intercept constrained to the origin, r^2=0.44, P=0.4, n=5). **(D)** The total concentration of probe was determined for muscle and tumor tissue samples from human (n=5) and mouse (n=18) STS subjects, using the equation: $[\text{Total Probe (nM)}]_{\text{tissue}}=[\text{LUM015 (nM)}]_{\text{tissue}}+[\text{Fragment 2 (nM)}]_{\text{tissue}}+[\text{Fragment 3 (nM)}]_{\text{tissue}}$. The concentration of total probe was significantly higher in tumors than normal muscle in the mouse cohort (P<0.0001, *t*-test, n=18), with a similar trend in the human cohort that did not reach statistical significance (P=0.08, *t*-test, n=5). **(E)** Tumor fluorescence is directly correlated with the concentration of total probe in the mouse and human STS cohorts (linear regression with y-intercept constrained to the origin, Human: r^2=0.18, P<0.05, Mouse: r^2=0.59, P<0.0001). **(F)** Tumor to muscle fluorescence ratios measured in mice injected with equimolar amounts of either LUM015 or LUM033, a constitutively active fluorescent imaging probe identical to Fragment 2 (P<0.05, *t*-test, n_{LUM015}=11, n_{LUM033}=9).

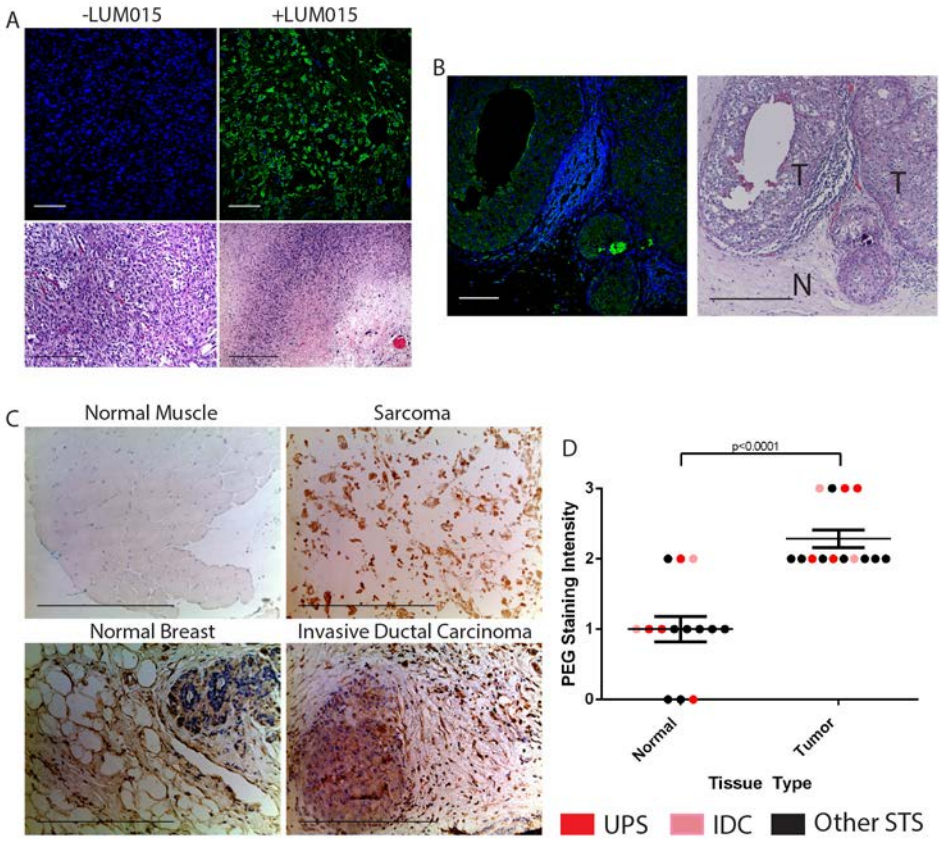

Figure 6

Figure 6: Immunofluorescent and immunohistochemical staining for the PEG moiety of LUM015 reveals a tumor-specific pattern. (**A**) PEG immunofluorescence of human tumor samples shows high signal in tumors from LUM015 injected patients (+LUM015 representative image from patient #2) with no signal detected in a tumor from an uninjected patient (-LUM015) with UPS. Blue, DAPI; green, PEG. (**B**) PEG immunofluorescence of formalin-fixed paraffin embedded margin tissue from LUM015 injected breast cancer patient #15, shows more intense PEG signal in areas that correspond with tumor (T) and less intense staining in areas of adjacent normal tissue (N). The corresponding hematoxylin and eosin stained section is shown below. Blue, DAPI; green, PEG. (**C**) Immunohistochemistry for PEG reveals minimal staining in normal muscle tissues, moderate staining of normal breast tissue, and the most intense staining in

tumor tissues. Representative images of normal muscle and undifferentiated pleomorphic sarcoma (patient #2) as well as normal breast and invasive ductal carcinoma (patient #9). (**D**) PEG staining intensity is significantly higher in tumors than in normal tissues ($P<0.0001$, Mann Whitney test, data includes 1 tumor and 1 normal tissue sample from each patient except patient 10 where no tumor sample was available). Scale bars= 100 μm for immunofluorescence images and 500 μm for immunohistochemistry and H&E images.